Short-range structural properties of $Nd_{1.85}Ce_{0.15}CuO_4$ and Nd_2CuO_4 studied by multiple-scattering EXAFS data analysis

Francesco Sperandini and Andrea Di Cicco
Dipartimento di Matematica e Fisica, Università degli Studi di Camerino, Istituto Nazionale di Fisica della Materia, Via Madonna delle Carceri, 62032 Camerino (MC), Italy

Maria Gazda
Wydzial Fizyki Technicznej i Matematyki Stosowanej, Politechnika Gdanska, Narutowicza 11/12, 80 952, Gdansk, Poland
(Received 14 February 1997; revised manuscript received 13 June 1997)

An accurate multiple-scattering Cu *K*-edge extended x-ray-absorption fine-structure (EXAFS) study of the average local structure of $Nd_{1.85}Ce_{0.15}CuO_4$ and Nd_2CuO_4 is presented in the range of temperature 5–150 K. Clear differences between experimental EXAFS signals of doped and undoped compounds recorded at the same temperature are found. Shortening of 0.015 Å of the average Cu-Nd/Ce distance is unambiguously detected in the doped-superconducting compound. We show that the contraction of the unit cell along the *c* direction can be assigned to the shift of the Nd/Ce atoms toward the adjacent CuO_2 plane. No evidence for anomalies of the in-plane Cu-Cu and Cu-O distance distribution is found as a function of temperature and doping. The strong multiple-scattering signal associated with the quasilinear Cu-O-Cu chains in the CuO_2 planes is used to evaluate the angle distribution at the oxygen site, using a suitable model describing a realistic three-atom vibrating system. Differences between the doped and the undoped compound are detected showing that the angle distribution is broader below T_c in the doped compound. The increased width of the angle distribution is consistent with the existence of local modes or permanent structural distortions involving the in-plane oxygens. [S0163-1829(98)01109-6]

I. INTRODUCTION

Since its discovery by Tokura *et al.* in 1989,[1] the $Nd_{2-x}Ce_xCuO_{4-\delta}$ (NCCO) compound has played an important role in the high-T_c superconductor research field, due to the nature of the charge carriers (electrons). Moreover, these cuprates crystallize according to a tetragonal T' structure, differently from other families of *T*-phase high-T_c superconductors, like $La_{2-x}(Ba/Sr)_xCuO_{4-\delta}$ or $YBa_2Cu_3O_{7-\delta}$ (see, for example, Ref. 2).

The existence of a strong interplay between superconducting properties and crystal structural distortions, defects, or local vibrational properties in high-T_c superconductor cuprates is well known.[3,2] Considerable effort has been devoted to study structural and vibrational properties of neodymium cuprates. Changes in the unit-cell parameters as a function of doping have been studied by several authors (see, for example, Refs. 4,5). Some studies using x-ray, neutron-diffraction,[6,5] and Raman[7] spectroscopy reported evidence of structural distortions and coexistence of phases in NCCO due to the presence of the dopants. In particular, the CuO_2 planes were found to be buckled due to in-plane and out-of-plane oxygen atom displacements.[6] Furthermore, various techniques including neutron-diffraction and infrared reflectivity spectroscopy showed evidence for polaron formation in this class of compounds, associated with local modes involving the in-plane oxygens (see Refs. 8,9,6 and references therein).

X-ray-absorption spectroscopy (XAS), due to its extremely high sensitivity to the short-range structure, can provide an important tool to study local structural properties in this class of cuprates. However, it should be stressed that, in presence of inhomogeneities in the local structure, an unpolarized XAS study rather provides information on the average short-range structure around a selected atomic site. In this case, additional information obtained using different techniques are required for a complete structural characterization. A few extended x-ray-absorption fine structure) (EXAFS) studies have been carried out in neodymium cuprates, mainly using standard data-analysis techniques.[10–12] As an example, the existence of interstitial apical oxygens in the Nd_2CuO_y ($y\sim4$) crystal structure was suggested by EXAFS (Ref. 11) and neutron diffraction,[13] although other neutron-diffraction studies gave a negative answer.[14,6]

Unfortunately, previous EXAFS studies on high-T_c cuprates, have rarely been recognized to give reliable structural information complementing that obtained by other spectroscopies. However, these studies were mainly conducted using standard data-analysis techniques which hardly provide reliable information beyond the first-neighbor shell.

Modern EXAFS data-analysis methods,[15–17] using multiple-scattering (MS) theoretical approaches, offer the possibility of a reliable investigation of the short-range structure. In this way, we are able to obtain quantitative evaluation of bond lengths, bond angles, and related variances associated with thermal motion and configurational disorder.[17] In particular, experimental determination of the short-range pair and triplet distribution functions around copper, which can be obtained by MS-EXAFS data analysis, can give us important information about structural distortions in cuprates.

In this work an accurate MS-EXAFS data analysis at the Cu *K* edge of Nd_2CuO_4 (NCO) and $Nd_{1.85}Ce_{0.15}CuO_4$ (NCCO) is performed, using the recently developed GNXAS method.[17,18] This method includes accurate modeling of

atomic background and MS contributions, providing also rigorous statistical analysis of the structural results.[17,18] The EXAFS spectra of layered cuprates invariably contain large multiple-scattering signals associated with the Cu-O-Cu in-plane linear configuration[19–21] (focusing effect[22]). As previously reported, MS-EXAFS data analysis can provide reliable information on the Cu-O-Cu angle distribution, directly related to the local corrugation of the CuO_2 plane.[20,21] Moreover, due to the strong backscattering signals related to Nd and Ce atoms, the EXAFS result to be particularly sensitive to possible displacements of these atoms from their crystallographic positions. The aim of this work is to obtain new information about the average local structure around Cu as a function of temperature, doping, and about the nature of the above-mentioned structural distortions, taking into proper account the context of published neutron diffraction and other spectroscopic data.

The paper is organized as follows: in Sec. II XAS experiments on neodymium cuprates are presented and analyzed at a qualitative level; in Sec. III details concerning the multiple-scattering data analysis of XAS measurements of cuprates are reported; results of the present work are discussed in Sec. IV, while in Sec. V the main conclusions of this work are resumed.

II. EXPERIMENTAL EVIDENCES

Well-characterized powders[23] of Nd_2CuO_4 and $Nd_{1.85}Ce_{0.15}CuO_4$ obtained using standard preparation methods[1,4] were used to prepare samples suitable for XAS measurements. X-ray diffraction and ac susceptibility measurements were performed showing the expected structural and conduction properties in these compounds (onset T_c = 19 K). The method and the procedure for XAS sample preparation are identical to that reported in the experimental section of Ref. 21. The samples are pellets with a diameter about 13 mm and thickness about 1 mm, obtained by mixing the powders with appropriate amounts of boron nitride.

XAS data collection was performed in transmission mode at LURE (Laboratoire pour L'Utilisation du Rayonnement Electromagnetique) on D21 beamline using Si(311) monochromator and harmonics rejecting mirrors. Low-temperature measurements from 5 to 150 K were performed with a He flux cryostat. In Fig. 1 the experimental $k^2\chi(k)$ as a function of the photoelectron wave vector $k \sim \sqrt{E-E_e}$ (where E_e is the experimental threshold energy) in the range of temperature between 5 and 150 K, are compared. The extraction method of the EXAFS oscillations from the raw data (x-ray-absorption coefficient at the Cu K edge) will be illustrated in the next sections. Measurements are characterized by a very low statistical noise level (of the order of 10^{-4}) and a quite large energy range (up to $k \sim 18.5$ Å^{-1}) at low temperatures. Clear differences between doped and undoped compound are easily detected.

The main differences are confined in the photoelectron wave-vector k interval between 10 and 15 Å^{-1}. This region of the spectrum is substantially dominated by the high-frequency Cu-Nd signal and the strong multiple-scattering contribution coming from Cu-O-Cu linear configurations in the CuO_2 plane (focusing effect). The attenuation of the structural signal obtained increasing the temperature is clearly visible at high k values, as expected.

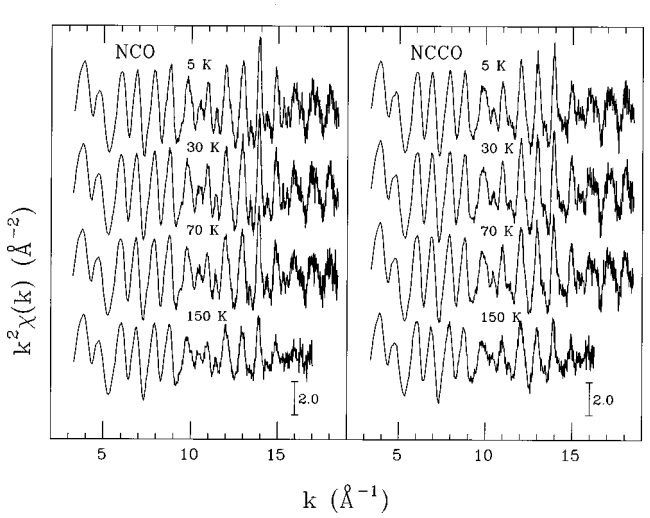

FIG. 1. Experimental $k^2\chi(k)$ signals for NCO (left panel) and NCCO (right panel) in the 5–150 K temperature range.

Fourier transforms (FT) of experimental $k^2\chi(k)$ for either NCO and NCCO for all of the investigated temperatures are reported in Fig. 2. Several well defined peaks corresponding to interatomic distances between the Cu atom (photoabsorber) and atoms belonging to the near coordination shells (backscattering atoms) are visible up to a distance of about 8.0 Å. According to the published crystal structure,[1] the nearest-neighbor atoms are: In-plane oxygens (CuO_2 plane) with coordination number $N=4$ at 1.97 Å (first coordination shell), Nd with $N=8$ at 3.33 Å (second coordination shell),

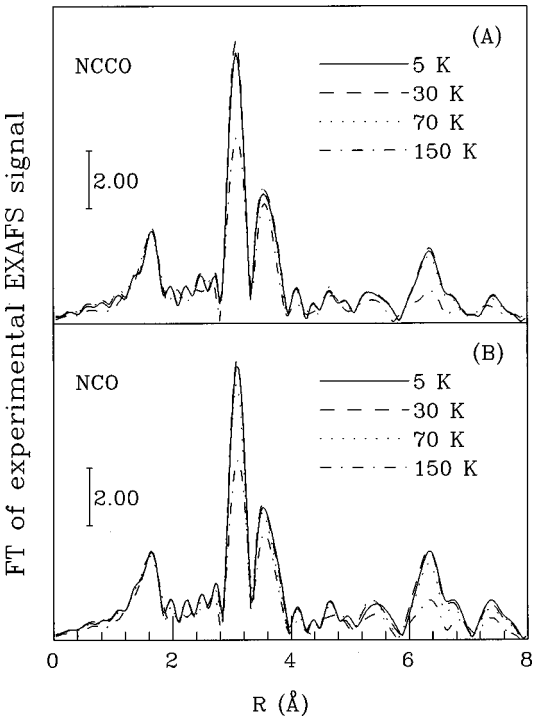

FIG. 2. Fourier transform of the $k^2\chi(k)$ for NCCO (panel A) and NCO (panel B) in the 5–150 K temperature range.

O(2) (out-of-plane oxygen) with $N=8$ at 3.63 Å Cu with $N=4$ at 3.95 Å. Taking into account the negative phase-shift contribution, the FT peaks follow the succession of coordination shells. The first peak at about 1.6 Å is related to the in-plane oxygens; the second peak, which is the biggest one, is associated with the Nd shell of atoms. Looking at the crystal structure it is clear that the third peak at about 3.6 Å in Fig. 2 is due to both Cu-Cu and Cu-O(2) contributions. However the contribution from the O(2) is very weak and this peak is largely dominated by the MS Cu-O-Cu contribution in the focusing configuration. Another prominent peak at about 6.35 Å is mainly due to another shell of 16 Nd atoms at 6.5 Å. The last peak at about 7.4 Å is related to the presence of Cu atoms at about 7.9 Å in the Cu-O-Cu-O-Cu in-plane configurations. Again, in spite of the large distance from the photoabsorber, the relatively large amplitude of this peak is related to the enhancement of the multiple-scattering signal in linear atomic configurations.

The trend of the magnitude of the FT peaks as a function of temperature is slightly different for the two compounds, as shown in Fig. 2. In particular, we observe a reduction of the height of the Cu-Nd/Ce peak (second peak) going from 30 K (dashed line, above T_c) to 5 K (solid line, below T_c). This effect is much less evident in the undoped compound. Being the magnitude of the peaks directly related to the vibrational amplitudes or to the static disorder of the atoms pair, this occurrence suggests that the presence of the dopant contributes to increase the structural disorder in the superconducting phase, with respect to the insulating one. We also observe a similar behavior in the third peak (panel A) related to the collinear configuration Cu-O-Cu in NCCO, absent in the undoped compound.

Even more interesting is the analysis of the differences between the doped and undoped compounds at fixed temperature. A simple subtraction between EXAFS spectra at the same temperature is able to highlight the main differences related to the local structure of the two compounds. This is especially interesting below the critical temperature of the doped compound NCCO. In Fig. 3 (upper panel) we report the experimental $k^2\chi(k)$ at $T=$ 5 K for NCCO and NCO. The result of the subtraction $k^2\Delta\chi(k) = k^2\,[\chi(k)_{\mathrm{NCCO}} - \chi(k)_{\mathrm{NCO}}\,]$ is shown in the middle panel of the same figure on the same scale of the starting signals. For the other temperatures we obtained similar results. As mentioned above the difference becomes quite large starting from $k=10$ Å^{-1}, but now one can see differences in the full range of the measurement associated with well defined frequencies. A Fourier transform of the difference spectrum (Fig. 3, lower panel) shows the main contributions to the total $k^2\Delta\chi(k)$ in the R space.

The main peak in the FT of the difference spectrum can be unambiguously assigned to differences in the Cu-Nd/Ce contribution, related to variations of the Cu-Nd/Ce distance distribution. The smaller peak at about 6.35 Å can be assigned to variations of the distant shell Cu-Nd/Ce contribution, and therefore give us essentially the same information. The last important peak at about 7.4 Å is associated with variations of the high-frequency signal related to the Cu-O-Cu-O-Cu chains, as previously mentioned. Differences are much less pronounced in the region 3.6–4 Å where variations of Cu-O-Cu distribution should also give a contribution. However, the vicinity of the huge Cu-Nd/Ce peak, generating ripples in the FT, could complicate the interpretation of this region of the difference spectrum. As a matter of fact, the Cu-O-Cu-O-Cu MS signal is much more sensitive to deviations from linearity of the chain than the corresponding signals due to both the three-atom Cu-O-Cu and O-Cu-O configurations, as it can be shown by direct calculation. Therefore, the presence of the peak around 7.4 Å in the difference spectrum is by itself an indication that in-plane Cu-O-Cu configurations are perturbed by the presence of the dopant.

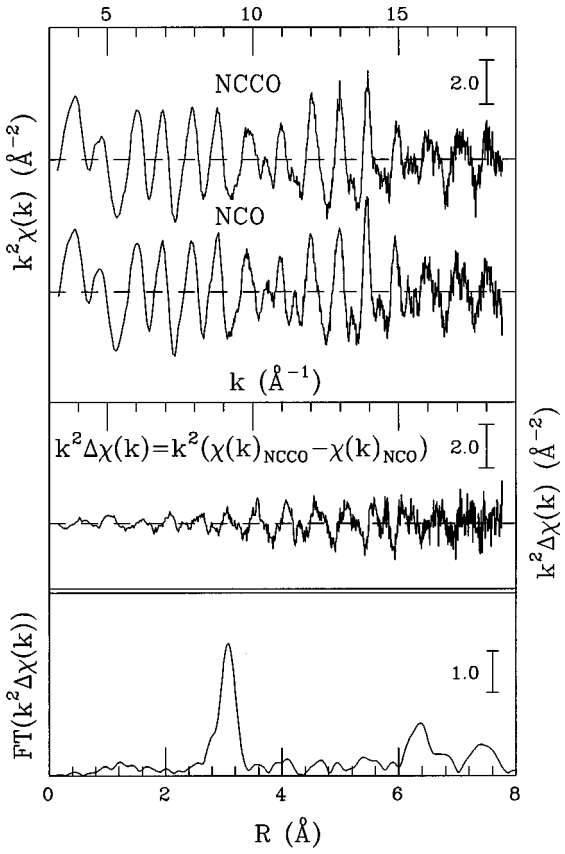

FIG. 3. Upper panel: Comparison between NCCO and NCO experimental EXAFS $[k^2\chi(k)]$ signal. The dashed line indicates $\chi(k)=0$. Middle panel: Difference EXAFS spectrum $k^2\Delta\chi(k)$ between doped and undoped compound related signals. Lower panel: Fourier transform of the difference spectrum.

These experimental evidences indicate the local structure in doped and undoped compounds are remarkably different and these differences can be easily revealed by EXAFS. At this point, in order to proceed in the quantitative interpretation of the EXAFS data we need to use modern EXAFS data-analysis methods taking proper account of the strong multiple-scattering contributions to the total EXAFS signal. The next sections are devoted to elucidate the methodology and report the results of the data analysis.

III. MULTIPLE-SCATTERING DATA ANALYSIS

Multiple-scattering (MS) EXAFS data analysis was performed using the GNXAS method.[17,18] In this section we introduce the fundamental aspects of the method with reference only to the specific case under consideration, referring

for the details to the original papers (see Refs. 17,18 and references therein).

The method is based on a comparison between the experimental absorption coefficient $\alpha_{\rm exp}(E)$ and the theoretical model of absorption, calculated according to equation

$$\alpha_{\rm mod}(E)=\alpha_0(E)[1+S_0^2\chi_{\rm mod}(E-E_0)]+\alpha_{bgk}(E)+\alpha_{\rm exc}(E), \quad (1)$$

where $\alpha_0(E)$ is the atomic absorption, $\alpha_{bgk}(E)$ is a smooth polynomial function taking into account underlying absorption channels, $\alpha_{\rm exc}(E)$ accounts for possible multielectron excitation channels, and $\chi_{\rm mod}(E-E_0)$ is the structural EXAFS signal. E_0 defines the energy scale of the theoretical signal (corresponding within a few eV to the edge energy), and S_0^2 is an amplitude correction factor ranging usually between 0.8 and 1.

Particular attention was paid to the background modeling in order to perform an accurate quantitative EXAFS data analysis. In a recent paper[21] about the study of local structural properties of $La_{1-x}(Sr/Ba)_xCuO_4$ the existence in the absorption background of an important $\alpha_{\rm exc}(E)$ contribution due to the presence of $[1s3p]$ double-electron excitation channels was pointed out. In the present work, we used the background shape observed in Ref. 21 for this $[1s3p]$ channel.

The model $\chi_{\rm mod}(k)$ was calculated as a sum of the two-body $\gamma^{(2)}$ and three-body $\gamma^{(3)}$ MS signals associated with the local n-atom configurations including the photoabsorber (Cu in our case). The $\gamma^{(2)}$ and $\gamma^{(3)}$ signals are oscillating functions in the k space. The $\gamma^{(2)}$ terms are associated with pairs of atoms and probe bond lengths and bond variances; the $\gamma^{(3)}$ functions, associated with triplets of atoms, probe bond angles, bond-bond, and bond-angle correlations.

Due to the short mean free path of the ejected photoelectron ($\sim 5-10$ Å) a limited number of irreducible $\gamma^{(n)}$ terms is sufficient to calculate the model EXAFS signal. In the present analysis only $\gamma^{(2)}$ and $\gamma^{(3)}$ signals were used in the model $\chi_{\rm mod}(k)$ calculation, reproducing the experimental features up to about 4 Å (cutoff distance) from the photoabsorber. The $\gamma^{(n)}$ signals were calculated using the muffin-tin approximation with an overlap of about 10% between nearest atomic spheres and using a Hedin-Lundqvist complex exchange-correlation potential.[17]

In Fig. 4 (upper panel) MS $\gamma^{(2)}$ and $\gamma^{(3)}$ irreducible signals calculated for the NCO compound are shown. A total of six $\gamma^{(n)}$ signals, associated with the main two-body and three-body atomic configurations up to a distance of 4 Å from the Cu site, are reported. They are, from the top to the bottom of Fig. 4 (upper panel): the first-neighbor $\gamma^{(2)}$ Cu-O signal related to the in-plane oxygens at 1.97 Å; the Cu-O(2) two-body contribution related to the out-of-plane oxygens at 3.63 Å; the strong high-frequency Cu-Nd $\gamma^{(2)}$ signal; the important three-body term associated with the linear Cu-O-Cu in-plane configurations; the in-plane two-body Cu-Cu contribution, and the three-body Cu-O-Nd signal involving in-plane oxygens. All of the signals include thermal factors specified in the next section.

Notice the clear difference in frequency between the Cu-O signal (low frequency) and the signals related to the other outer coordination shells (high frequency). Both the low- and high-frequency signals contribute to determine the Cu-O distribution. In fact, the Cu-O-Cu signal ($\gamma^{(3)}$) is about three times larger than the Cu-Cu ($\gamma^{(2)}$) one, as expected, due to the focusing configuration. The proper inclusion of the Cu-O-Cu signal allows us to determine more accurately the Cu-O distance distribution. We remark that the common procedure used to treat the focusing contribution, i.e., the use of an artificial increase of the Cu-Cu coordination number, cannot work properly because the Cu-O-Cu MS signal has a different phase with respect to the Cu-Cu two-body one.

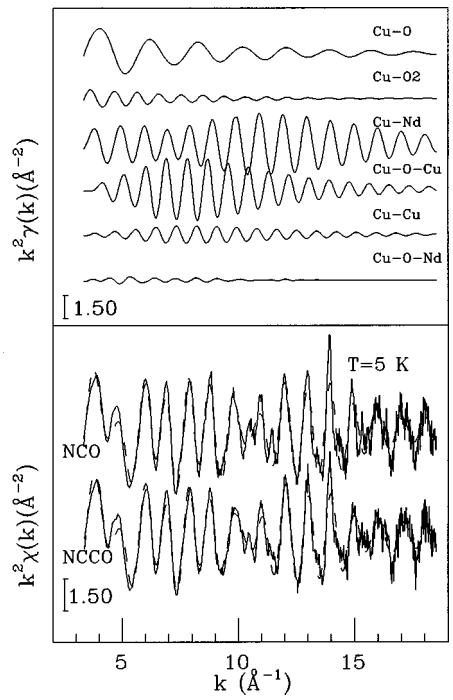

FIG. 4. Upper panel: MS $k^2\gamma^{(n)}$ signal associated with the main two-atom and three-atom configuration contributing to the total $k^2\chi(k)$. Lower panel: Experimental (solid curve) and model (dashed) $k^2\chi(k)$ for NCO and NCCO at 5 K.

In the same figure (lower panel) we report the fitting results at $T=5$ K for both the compounds under consideration. The experimental EXAFS signal $k^2\chi(k)$ was obtained by subtracting the best-fit atomic background function $\alpha_{bgk}(E)+\alpha_{\rm exc}(E)$ to the raw data $[\alpha_{\rm exp}(E)]$ and using a hydrogenic model for the K-edge atomic absorption as a normalizing factor. The small discrepancy in the second peak at $k\sim 4.7$ Å is due to the difficulty in the proper modeling of the onset of the $[1s3p]$ double-electron excitation channel. In any case, all the experimental features are quite accurately reproduced in the entire range of investigated temperatures.

In the framework of the GNXAS method, the evaluation of best-fit structural parameters and their statistical errors is performed by minimizing the differences between experimental and model absorption, using a square residual function:

$$R(\{\lambda\})=\sum_{i=1}^{N}\frac{[\alpha_{\rm exp}(E_i)-\alpha_{\rm mod}(E_i,\lambda_1,\lambda_2,\ldots,\lambda_p)]}{\sigma_i^2}, \quad (2)$$

where $\{\lambda\}=(\lambda_1,\lambda_2,\ldots,\lambda_p)$ indicates the set of p parameters on which $\alpha_{\rm mod}$ depends. Each energy point E_i of the

experimental signal is assumed to be affected by random Gaussian noise with standard deviation σ_i.

Following the standard statistical theory[18] it is possible to evaluate the optimal values of the fitted parameters finding those values, $\{\lambda\}=\{\overline{\lambda}\}$ that minimize the residual function. The correlated errors on the structural parameters can be evaluated looking at the confidence intervals defined by the equation

$$R(\{\lambda\})<R_{\min}+C, \tag{3}$$

where C, depending upon the number of the p free parameters, defines the confidence interval.

In this analysis six structural parameters were floated: $R_{\text{Cu-O}}$, $R_{\text{Cu-Nd}}$, $\sigma^2_{\text{Cu-O}}$, and $\sigma^2_{\text{Cu-Nd}}$ interatomic distances and variances; the Cu-O-Cu angular deviation δ_θ (see the next section) and the bond-bond ρ_{RR} correlation used to parametrize the Cu-O-Cu distribution. The other structural quantities are associated with minor multiple-scattering contributions and were fixed to the corresponding crystallographic values. Explicit introduction of the Cu-Ce and Cu-O-Ce contributions were shown to be useless to improve the quality of the fit. Those contributions were grouped with the corresponding Cu-Nd and Cu-O-Nd ones. Moreover, introduction of asymmetric distance Cu-Nd/Ce distribution by using Γ-like functions or the cumulant expansion was found not to lead to statistically significant improvements of the fitting results. Therefore, a total number of eight parameters ($p=8$) was used in the fitting procedure, the six structural parameters mentioned above plus the E_0 and S_0^2 parameters defined in Eq. (1). The energy E_0 resulted to be 8994 (1) eV for NCCO and 8995 (1) eV for NCO, while we found $S_0^2\sim 0.96$ in all cases. The residual function defined in Eq. (2) follows the χ^2 distribution with p degrees of freedom,[18] therefore for a 95% confidence interval, we find $C=15.5$.

The contour plots associated with $R_{\text{Cu-O}}$ (upper panel) and $R_{\text{Cu-Nd}}$ (lower panel) versus E_0 at $T=30$ K are reported in Fig. 5, upper and center panels. The inner elliptical curves correspond to the intersection of the 95% p-dimensional confidence interval with the particular two-parameter plane. E_0 and bond distances are found to be strongly correlated, as usual. On the other hand, bond variances are mainly correlated with the S_0^2 amplitude factor, as expected. From contour plots we infer the statistical errors on the structural parameters including correlation with the other variables. For example, in Fig. 5, lower panel, we report the contour plots associated with $R_{\text{Cu-Nd}}$ and δ^2_θ, which result to be practically uncorrelated. Two-dimensional contours are especially interesting for parameters which are found to be very correlated in order to get the more realistic estimates for statistical errors. In this way, a statistical error of about 0.004 Å on the Cu-O and Cu-Nd distances is found looking at Fig. 5. Error in the angular deviation δ_θ as determined by Fig. 5, lower panel, resulted to be around 1°.

As a final comment about the data analysis we would like to remark that high-frequency contributions (effective distance $R>4$ Å) not explained by the present theoretical model have not dramatic consequences on the statistical evaluation of the results. In fact, the minimum of the residual function results simply translated by a residual associated with the high-frequency components.[18]

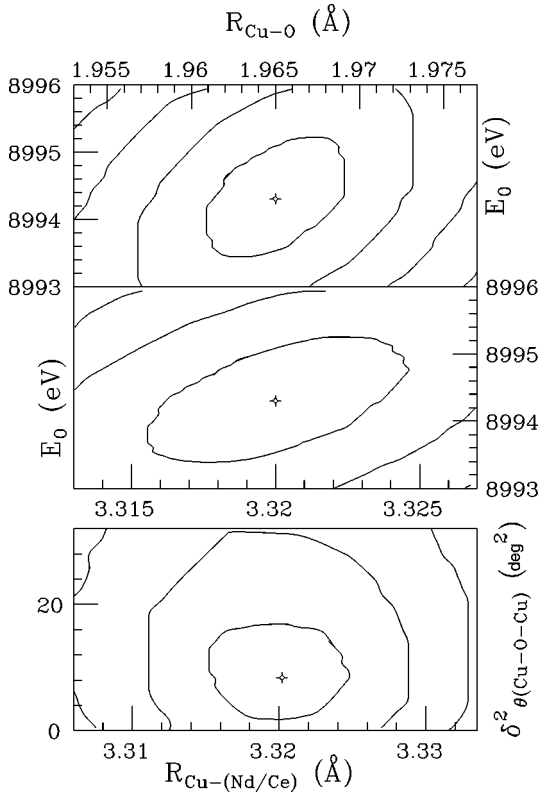

FIG. 5. $R_{\text{Cu-O}}$-E_0, $R_{\text{Cu-Nd}}$-E_0, and $R_{\text{Cu-Nd}}$-δ^2_θ contour maps derived by EXAFS data analysis. The inner elliptically shaped curves represent the 95% (2σ) confidence interval.

IV. RESULTS AND DISCUSSION

As a result of the above-mentioned data-analysis methodology, we obtained the best-fitting models $\chi_{\text{mod}}(k)$ as a function of temperature for the two compounds under consideration.

Let us first consider the difference between the EXAFS spectra of the doped and undoped compounds at $T=5$ K, for which qualitative considerations have been anticipated in Sec. II (see Fig. 3). In Fig. 6 (upper panel) the two theoretical $k^2\chi_{\text{mod}}(k)$ are reported and superimposed to highlight their phase and amplitude differences. The difference spectrum $k^2\Delta\chi_{\text{mod}}(k)$ (solid line) is also reported below and compared with the experimental difference spectrum of Fig. 3 (dashed line). Our models are therefore able to reproduce very accurately also the relatively small differences found between NCO and NCCO EXAFS spectra.

FT spectra of the model (solid line) and experimental (dashed line) $k^2\Delta\chi(k)$, reported in Fig. 6 (lower panel), confirm that the main differences between doped and undoped compound can be unambiguously assigned to changes in the Cu-Nd/Ce distance distribution. Similar results were found for the other investigated temperatures.

Best-fitting Cu-O, Cu-Nd, and Cu-Cu interatomic average distances and variances for NCCO and NCO as a function of temperature are reported in Table I. The $R_{\text{Cu-Cu}}$ and $\sigma^2_{\text{Cu-Cu}}$ bond distances and variances have been evaluated as a function of the floating parameters defining the Cu-O distance Cu-O-Cu angle distributions, following methods reported in Ref. 18. The results about the Cu-Nd/Ce average distance reveal that there is a contraction of about 0.015 Å for the

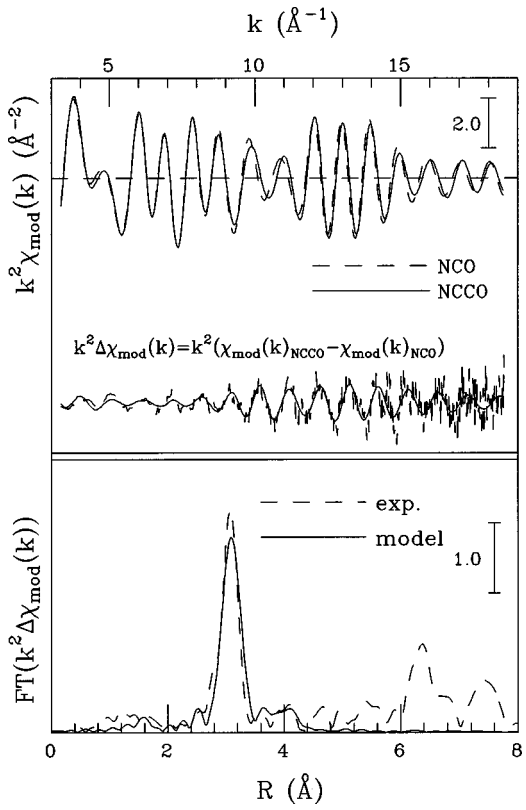

FIG. 6. Upper panel: Comparison between best-fitting model $k^2\chi(k)$ for NCO (dashed) and NCCO (solid) at 5 K. Below, the comparison between experimental (dashed) and model (solid) difference spectra is reported. Lower panel: Fourier transform of experimental (dashed) and model (solid) difference spectra.

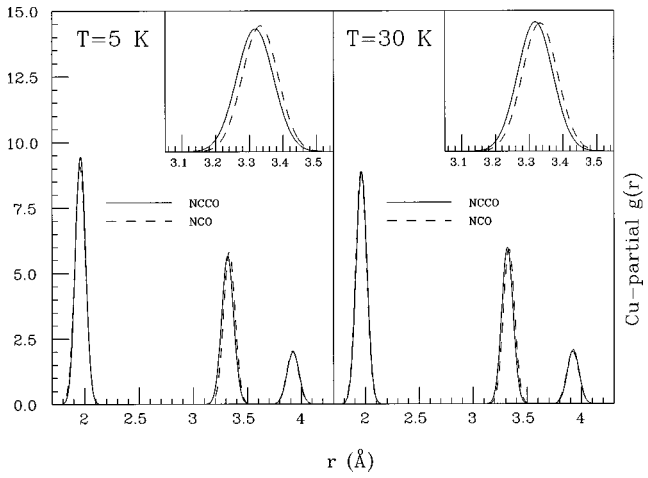

FIG. 7. Cu partial radial distribution function $g(r)$ for NCCO (solid) and NCO (dashed) at 5 K (left panel) and 30 K (right panel). A magnification of the difference between doped and undoped compound in the Cu-Nd related peaks is reported in the insets.

doped compound, in the full range of temperatures. Distance variances are found of the same order of magnitude in both cases, although a slight anomalous increase at $T=5$ K for NCCO is found. These results can be compared with recent pair-density function (PDF) analysis of neutron powder-diffraction measurements of NCCO,[6] where small displacements of Nd/Ce atoms from their crystallographic positions (less than 0.03 Å) were reported. In that study, these displacements were considered deviations contained within the thermal motion of atoms. From the local point of view provided by EXAFS, the shift of 0.015 Å in the Cu-Nd/Ce distance is measured with high accuracy and cannot be confused with the thermal motion, which is related with the distance variance, also accurately measured.

On the other hand, $R_{\text{Cu-O}}$ and $R_{\text{Cu-Cu}}$ distances are found to be in a good agreement with the results obtained with diffraction techniques.[24,6,13] The Cu-O variances are in substantial agreement with those estimated using a simple Einstein model with the Cu-O stretching frequency $\omega_{\text{Cu-O}} \sim 513$ cm^{-1}, measured in NCO by infrared spectroscopy.[25] The calculated bond variance at $T=5$ K resulted to be $\sigma^2_{\text{Cu-O}} \sim 0.0026$ Å^2. The structural parameters reported in Table I have been used to reconstruct the Cu partial distribution function $g(r)$ (calculated using the atomic density $\rho = 0.0743$ Å^{-3}). In Fig. 7 we report the comparison between calculated $g(r)$ distributions for NCO (dashed) and NCCO (solid) at $T=5$–30 K. Notice that the Cu-O (first peak) and Cu-Cu (third peak) average distances are basically not influenced by doping with Ce. No significative statistical correlations have been observed between Cu-Nd/Ce structural parameters and the in-plane Cu-O-Cu ones (see, for example, Fig. 5, lower panel). For sake of clarity, the Cu-O(2) (out-of-plane oxygen) distance distributions is not reported in the figure. The two insets in Fig. 7 show a magnification of the differences in the second peak of the $g(r)$ related to the Cu-Nd/Ce interatomic distance.

TABLE I. Best-fitting structural parameter values as function of temperature for NCCO and NCO. Numbers in parentheses are statistical errors of the last significant digit.

	T (K)	$R_{\text{Cu-O}}$ (Å)	$\sigma^2_{\text{Cu-O}}$ (Å^2)	$R_{\text{Cu-Nd}}$ (Å)	$\sigma^2_{\text{Cu-Nd}}$ (Å^2)	$R_{\text{Cu-Cu}}$ (Å)	$\sigma^2_{\text{Cu-Cu}}$ (Å^2)
NCCO	5	1.964(4)	0.0022(8)	3.319(4)	0.0030(4)	3.925(8)	0.0031(8)
	30	1.965(4)	0.0025(8)	3.320(4)	0.0027(4)	3.926(8)	0.0029(8)
	70	1.964(4)	0.0023(8)	3.321(4)	0.0029(4)	3.926(8)	0.0030(8)
	150	1.963(5)	0.0025(9)	3.324(6)	0.0045(5)	3.92(1)	0.0035(9)
NCO	5	1.961(4)	0.0024(8)	3.334(4)	0.0028(4)	3.921(8)	0.0030(8)
	30	1.961(4)	0.0025(8)	3.334(4)	0.0027(4)	3.922(8)	0.0031(8)
	70	1.963(4)	0.0026(8)	3.335(4)	0.0032(4)	3.923(8)	0.0032(8)
	150	1.962(5)	0.0029(9)	3.337(6)	0.0047(5)	3.92(1)	0.0041(9)

The change in the $R_{\text{Cu-Nd}}$ distance distribution obtained introducing Ce atoms in the structure of Nd_2CuO_4 deserves some considerations. In the T' crystal structure the Nd atoms are located along the direction defined by the c axis, above (and below) the center of squares (belonging to the CuO_2 planes) having the Cu atoms at the corners and in-plane O atoms in the center of each side. A generic Cu atom has eight Nd neighbors at the same distance of about 3.33 Å. Simple symmetry considerations suggest that the Nd/Ce displacement occurs in the perpendicular direction (d_z) towards the CuO_2 plane. On the contrary a d_{xy} displacement, parallel to the CuO_2 planes, would result in a broader Cu-Nd/Ce distribution, or even in a splitting of distances for the doped compound, ruled out by present investigation. According to this picture we can conclude that the introduction of the dopant produces a displacement $d_z \sim 0.026$ Å of the Nd atoms towards the CuO_2 planes. Therefore we find a shortening of the vertical side of the cage composed by the eight Nd atoms around copper of about 0.052 Å.

Therefore, our EXAFS analysis shows that the contraction of the unit cell in the c direction is related to the Nd/Ce displacement. According to the structure of the T' unit cell, we have to account for a total of four d_z displacement in the c direction, each one towards the nearest CuO_2 plane, resulting in a total shortening $\Delta c \sim 0.0026 \times 4 = 0.104$ Å. This value is already in very good agreement with the difference $\Delta c \sim 0.1$ Å between Nd_2CuO_4 and $Nd_{1.85}Ce_{0.15}CuO_4$ reported in the literature (see, for example, Ref. 4). In our local determination, the contraction of the c axis results to be due *only* to the shift of the Nd/Ce atoms towards the CuO_2 adjacent planes, without affecting the layer of oxygens, nearest neighbors of Nd and Ce atoms.

It is also interesting to remark that the slight increase of the $\sigma^2_{\text{Cu-Nd}}$ distance variance below 30 K, although practically contained within the statistical error bar (defined by the 95% confidence level), follows the anomalous slight decrease of the Cu-Nd FT peak of the experimental EXAFS spectrum (see Fig. 2). The effect of the increase of $\sigma^2_{\text{Cu-Nd}}$ for NCCO at $T = 5$ K can be easily verified looking at the insets of Fig. 7. The slight modifications in the average distance and variances below T_c in NCCO could be also evidenced by the difference spectrum $k^2\Delta\chi(k) = k^2\,[\chi(k)_{30\text{ K}} - \chi(k)_{5\text{ K}}]$, although in this case the relatively large statistical noise obtained in the subtraction procedure (two times the statistical noise of the raw data) makes it difficult to observe oscillations at large wave-vector values. The unfiltered difference spectrum is shown in Fig. 8, upper panel, showing a large statistical noise above 10 $Å^{-1}$. However, the Fourier transform of this signal, shown in Fig. 8, lower panel, presents a well-defined peak at about 3.2 Å slightly above the noise level (indicated approximately by the dot-dashed line in Fig. 8) which can be mainly assigned to changes in the Cu-Nd/Ce distribution below T_c. The intensity of that FT peak is nicely reproduced by the FT of the analogous $k^2\Delta\chi(k)$ signal obtained using multiple-scattering best-fit simulation.

The observed modifications of the Cu-Nd/Ce distribution, and in particular the shortening of the average distance between NCO and NCCO, could influence the structural and vibrational characteristics of the CuO_2 plane, drastically

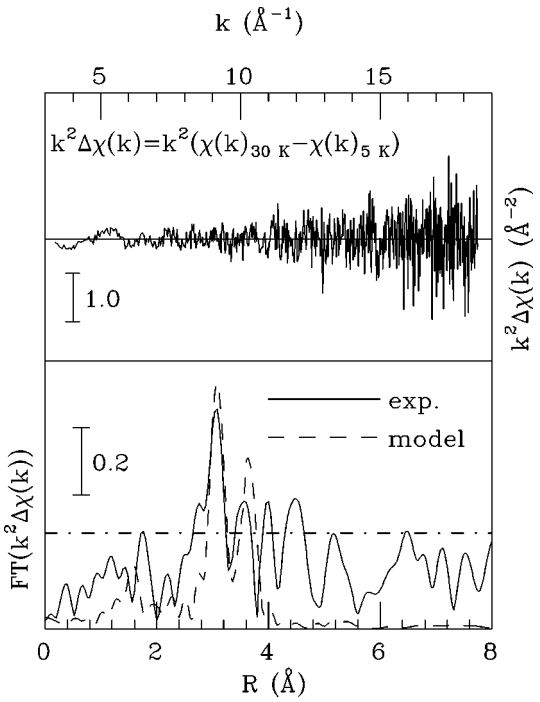

FIG. 8. Upper panel: Difference spectrum between experimental $k^2\chi(k)$ spectra of NCCO at 30 and 5 K. Notice the large statistical noise at high wave-vector values. Lower panel: Fourier transform of experimental (dashed) and model (solid) of difference spectra.

changing the conduction properties under T_c. A large debate is still open on the nature of structural distortion of the CuO_2 plane. Indeed it is not clear if the CuO_2 plane is locally buckled or it presents a long-range distortion in the crystal structure. In any case, no definitive results are still available (see Ref. 7 and references therein).

Previous EXAFS studies of layered superconductors cuprates showed that important multiple-scattering contributions associated with the Cu-O-Cu linear configuration in the CuO_2 plane can be successfully used to study the angular distribution in the Cu-O-Cu chains.[20,21] In lanthanum cuprates, for example, large deviations from collinearity for the Cu-O-Cu in-plane configuration were found, with average $\Delta\theta_{\text{Cu-O-Cu}} = 180 - \theta_{\text{Cu-O-Cu}}$ values of the order of 10° ($\theta_{\text{Cu-O-Cu}}$ is the angle measured at the oxygen site).[21]

In the NCCO and NCO systems, we found that significant shifts of the mean angle value from $\theta = 180°$ lead to an unacceptable poor agreement between experimental and calculated EXAFS signals. As it is well known, the first derivative of the MS three-body signals vanishes at $\theta = 180°$ and therefore we used a second-order derivative expansion to account for angle fluctuations around an average exactly linear Cu-O-Cu configuration (Ref. 18, and references therein).

The three-body distribution to be used for linear configurations needs some clarification.[18] In a real vibrating system composed by three aligned atoms (average positions of the in-plane Cu-O-Cu configuration in NCO and NCCO) the angular probability distribution vanishes at $\theta = 180°$. Distance and angular distributions can be factorized and a suitable model for the angle distribution function, depending only on the δ_θ parameter, can be written as

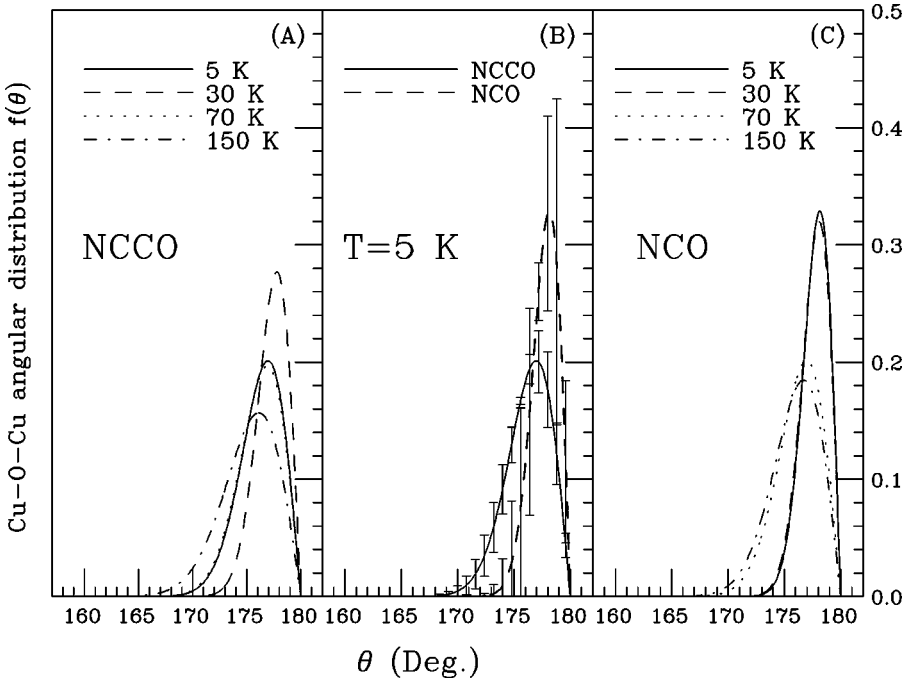

FIG. 9. Panels A and C: Angle distribution function $f(\theta)$ as a function of temperature for NCCO panel and NCO, respectively. Panel B: Comparison between $f(\theta)$ for NCCO (solid) and NCO (dashed) at 5 K. Error bars showing the accuracy of the present angle distribution determination are also shown.

$$f(\theta)=\frac{(180-\theta)}{\delta_\theta^2}\exp\left(-\frac{(\theta-180)^2}{2\delta_\theta^2}\right);0\leqslant\theta\leqslant180. \quad (4)$$

In absence of the linear term $(180-\theta)$, δ_θ^2 would be the angle variances around $\theta=180°$. The condition for vanishing probability at $\theta=180°$ implies a change in the shape of the distribution which has the maximum at $\theta_M=180°-\delta_\theta$. Therefore, the most probable angle value is always different from $\theta=180°$. For large angular fluctuations δ_θ, a disordered linear configuration ($\langle\theta_{\text{Cu-O-Cu}}\rangle=180°$) cannot be easily distinguished from a bent average configuration ($\langle\theta_{\text{Cu-O-Cu}}\rangle\neq180°$), but in the present case small values in the range $\delta_\theta=2°-5°$ have been found in the temperature range $T=5$–150 K.

In Fig. 9 (panel A and C) we report the best-fitting angular distribution function $f(\theta)$ in the range ($T=$ 5–150 K) for NCCO and NCO, respectively. Statistical error analysis showed that δ_θ is determined with an accuracy of about 1° (see Fig. 5, lower panel). As a consequence of this relatively large error bar, we can extract only qualitative information about the different behavior as a function of temperature between the doped and undoped compound as shown in Fig. 9. However, the trend as a function of temperature is very clear showing a broadening of the angular distribution for increasing temperature with the remarkable exception of NCCO at $T=5$ K.

The NCO angle distribution at 30 and 150 K is slightly narrower with respect to the NCCO one. However, there is a very slight difference at high temperature between NCO and NCCO angle distributions, suggesting that the structural disorder could be also related to the onset of the superconducting phase. Below the critical temperature, a larger δ_θ is found in the doped compound leading to a broader angle distribution (Fig. 9, panel B).

Unfortunately, the large statistical noise contained in the difference spectrum of Fig. 8 does not allow us to reveal unambiguously the change in the Cu-O-Cu distribution below T_c in NCCO using this simple self-evident procedure. The FT peak around 3.6 Å of the simulated signals (dashed line in Fig. 8, lower panel), representative of possible changes in the Cu-O-Cu distribution, is not found in the difference of experimental data (solid line in Fig. 8, lower panel). However, it is clear that these changes can be hidden by the relatively large noise of the difference experimental spectra. In fact, the statistical noise of the difference spectrum is two times larger than that of the original raw data and the FT spectrum (Fig. 8) contains many interfering peaks without direct structural meaning (the noise level is approximately indicated by the horizontal dashed line). In this case, possible changes in the Cu-O-Cu signal can be better revealed by studying the differences in the simulated best-fit signals which take into account the original data and not difference signals affected by a much larger noise.

Error bars showing the accuracy of the present determination of the angle distribution are reported in Fig. 9, panel B. Error bars are determined by propagation of errors analysis on δ_θ. In spite of the relatively large statistical error, significative portions of the angular distributions of NCO and NCCO at $T=5$ K are not overlapped. In particular, angle distribution in NCCO is different from zero for θ in the 170–175° range and has a lower intensity near 180°. In principle, this effect could be due both to different vibrational amplitudes and to static structural distortion (inhomogeneous local structure). Previously, experimental evidence supporting changes in local structure across T_c were also observed by

PDF analysis of neutron-diffraction data.[24] However, broadening of the NCCO angle distribution observed below T_c (panel A) rather suggests the activation of vibrational modes. The decrease of the Cu-O-Cu FT peak observed in NCCO at $T=5$ K (see Fig. 2) can be explained by this broadening.

Present results indicate that the local structural properties of NCCO and NCO are very different, as already shown by a preliminary analysis of the raw data reported in Sec. II. In particular, the evident shortening of the Cu-Nd/Ce distance in NCCO is accompanied by a broadening of the in-plane Cu-O-Cu angular distribution. Evidence for anomalous increase of the width of the angle distribution and of the Cu-Nd/Ce distance variance below T_c is found. Present estimates of the most probable angle value and width of the angle distribution are consistent with the in-plane oxygen vertical displacement of about 0.1 Å, as reported in Ref. 6. The broadening of the Cu-O-Cu angular distribution is definitely consistent with the presence of local vibrational modes involving in-plane oxygens. However, the existence of inhomogeneous local structure, compatible with present values of distance and angle variances, is not ruled out by present data. No evidence for variations of the Cu-O and Cu-Cu mean distances are found, differently from the results obtained for lanthanum superconductor cuprates, where clear changes of the in-plane average distances were found as a function of doping (see Ref. 21 and references therein). Moreover, no anomalous features for distance variances $\sigma^2_{\text{Cu-O}}$, $\sigma^2_{\text{Cu-Cu}}$ were found as a function of temperature. This occurrence suggests that local modes or permanent structural distortions, probably induced by the charge carried by the Ce dopant approaching the CuO_2 planes, are mainly associated with motion of oxygens perpendicular to the in-plane Cu-O bond direction.

V. CONCLUSIONS

The local structure around the Cu site in $Nd_{1.85}Ce_{0.15}CuO_4$ (NCCO) and Nd_2CuO_4 has been investigated in the range of temperature 5–150 K. Clear differences in the average local structural properties of the two compounds are evidenced in the raw data in the entire range of temperature under investigation.

Low-noise EXAFS data are analyzed using accurate *ab initio* multiple-scattering calculations finding that the spectra are particularly sensitive to the Cu-Nd/Ce distance distribution and to the in-plane Cu-O-Cu three-atom distribution. Statistical errors on the structural quantities are estimated showing that accurate short-range information can be derived by EXAFS in neodymium cuprates, providing that modern methods for data analysis are used.

The overall picture which emerges from our investigation can be summarized as: (i) the in-plane distance distributions Cu-O and Cu-Cu are not affected by doping and do not change appreciably in the 5–150 K range of temperature; (ii) the Cu-Nd/Ce distance distribution is strongly affected by doping and a shortening $\Delta R_{\text{Cu-Nd/Ce}} \sim 0.015$ Å is found in the doped compound; (iii) the in-plane Cu-O-Cu angle distribution is slightly broadened as a consequence of doping; (iv) broadening of the angle distribution is enhanced below T_c in the doped superconducting compound.

These results are consistent with previous studies showing a contraction of the *c* axis as a function of doping and with previously observed vertical displacements of the oxygen atoms (see Sec. IV). Distance variances are also in accord with vibrational modes measured by infrared spectroscopy. The shortening of the *c* side is fully explained in terms of the local displacement of the Nd/Ce atoms in the vertical direction, toward the adjacent CuO_2 planes. The reduction of the distance between the Nd/Ce atoms and the CuO_2 plane in the doped compound is found to be accompanied by an enhanced structural disorder on the same plane. This effect becomes more visible below T_c. This is quite remarkable, because changes in the angular distribution induced by doping could be associated with the onset of the superconducting phase. The broadening of the Cu-O-Cu angle distribution is assigned to variations in the local vibrational modes involving the in-plane oxygens, induced by doping. The absence of detectable changes in the Cu-O distance distribution suggests that those local modes are related to motion of oxygens perpendicular to the direction of the Cu-O bond. Formation of polarons surviving below T_c is therefore compatible with present evidence.

ACKNOWLEDGMENTS

We would like to thank Professor Sergio Stizza for his help during the experiments. This research was financed by Consiglio Nazionale delle Ricerche (Contract No. 96.00844.ST76), MURST and Istituto Nazionale di Fisica della Materia.

[1] Y. Tokura, H. Takagi, and S. Uchida, Nature (London) **337**, 345 (1989).
[2] W. E. Pickett, Rev. Mod. Phys. **61**, 433 (1989).
[3] K. Yvon and M. François, Z. Phys. B **76**, 413 (1989).
[4] H. Takagi, S. Uchida, and Y. Tokura, Phys. Rev. Lett. **62**, 1197 (1989).
[5] P. Lightfoot, D. R. Richards, B. Dabrowski, D. G. Hinks, S. Pei, D. T. Marx, A. W. Mitchell, Y. Zheng, and J. D. Jorgensen, Physica C **168**, 627 (1990).
[6] S. J. L. Billinge and T. Egami, Phys. Rev. B **47**, 14 386 (1993).
[7] M. A. Laguna, M. L. Sanjuán, A. Butera, M. Tovar, Z. Fisk, and P. Canfield, Phys. Rev. B **48**, 7565 (1993).
[8] P. Calvani, M. Capizzi, S. Lupi, and G. Balestrino, Europhys. Lett. **31**, 473 (1995).
[9] P. Calvani, M. Capizzi, S. Lupi, P. Maselli, A. Paolone, and P. Roy, Phys. Rev. B **53**, 2756 (1996).
[10] A. Yu. Ignatov, A. P. Menushenkov, A. A. Ivanov, and D. I. Kochubey, Physica C **234**, 68 (1994).
[11] P. Ghigna, G. Spinolo, A. Filipponi, A. V. Chadwick, and P. Hanmer, Physica C **246**, 345 (1995).
[12] P. Ghigna, G. Spinolo, M. Scavini, U. Anselmi Tamburini, and A. V. Chadwick, Physica C **253**, 147 (1995).
[13] P. G. Radaelli, J. D. Jorgensen, A. J. Schultz, J. L. Peng, and R. L. Greene, Phys. Rev. B **49**, 15 322 (1994).

[14] C. Marin, J. Y. Henryand, and J. X. Boucherle, Solid State Commun. **86**, 425 (1993).
[15] S. J. Gurman, J. Phys. C **21**, 3699 (1988); N. Binsted, J. W. Campbell, S. J. Gurman, and P. C. Stephenson, *SERC Daresbury Laboratory* EXCURV90 *program*, Daresbury Laboratory, Warrington WA4 4AD, England.
[16] J. Mustre de Leon, J. J. Rehr, S. I. Zabinsky, and R. C. Albers, Phys. Rev. B **44**, 4146 (1991); J. J. Rehr, J. Mustre de Leon, S. I. Zabinsky, and R. C. Albers, J. Am. Chem. Soc. **113**, 5135 (1991).
[17] A. Filipponi, A. Di Cicco, and C. R. Natoli, Phys. Rev. B **52**, 15 122 (1995). The acronym GNXAS derives from gn (the n-body distribution function) and XAS (x-ray absorption spectroscopy).
[18] A. Filipponi and A. Di Cicco, Phys. Rev. B **52**, 15 135 (1995).
[19] E. D. Crozier, N. Alberding, K. R. Bauchspiess, A. J. Seary, and S. Gygax, Phys. Rev. B **36**, 8288 (1987).
[20] A. Di Cicco and M. Berrettoni, Phys. Lett. A **176**, 375 (1993).
[21] A. Di Cicco and F. Sperandini, Physica C **258**, 349 (1996).
[22] B.-K. Teo, J. Am. Chem. Soc. **103**, 3990 (1981).
[23] M. Gazda, B. Kusz, R. Barczynski, O. Gzowski, L. Murawski, I. Davoli, and M. Berrettoni, Mater. Sci. Forum **119-121**, 695 (1993).
[24] S. J. L. Billinge, T. Egami, D. R. Richards, B. Dabrowski, D. G. Hinks, J. D. Jorgensen, and K. J. Volin, Physica C **179**, 279 (1991).
[25] S. Tajima, T. Ido, S. Ishibashi, T. Itoh, H. Eisaki, Y. Mizuo, T. Arima, H. Takagi, and S. Uchida, Phys. Rev. B **43**, 10 496 (1991).